Urban biowaste-derived sensitizing materials for caffeine photodegradation

Bianco Prevot, A; Baino, F.; Fabbri, D.; Franzoso, F.; Magnacca, G.; Nisticò, R.; Arques, A.. Urban biowaste-derived sensitizing materials for caffeine photodegradation. ENVIRONMENTAL SCIENCE AND POLLUTION RESEARCH INTERNATIONAL. None pp: 1-9.
DOI: 10.1007/s11356-016-7763-1

Urban biowaste-derived sensitizing materials for caffeine photodegradation

A. Bianco Prevot[1*], F. Baino[1], D. Fabbri[1], F. Franzoso[1], G. Magnacca[1,2], R. Nisticò[1], A. Arques[3]

[1]Università degli Studi di Torino, Dipartimento di Chimica and [2]NIS Centre, Via Giuria 7, Torino, Italy

[3]Universitat Politècnica de València, Dpto de Ingeniería Textil y Papelera, Plaza Ferrándiz y Carbonell s/n, Alcoy,Spain

*alessandra.biancoprevot@unito.it

+39 0116705292

Abstract

Caffeine photosensitized degradation has been studied in the presence of bio-based materials derived from urban biowaste after aerobic ageing. A peculiar fraction (namely BBSs), soluble in all the pH range, has been used as photosensitizing agent. Several caffeine photodegradation tests have been performed and positive results have been obtained in the presence of BBSs and H_2O_2, without and with additional Fe(II) (photo-Fenton-like process). Moreover hybrids magnetite-BBSs nanoparticles have been synthesized and characterized, in order to improve the sensitizer recovery and re-use after the caffeine degradation. In the presence of such nanoparticles and H_2O_2 and Fe(II), the complete caffeine degradation has been attained in very short time. Both homogeneous and heterogeneous processes were run at pH = 5, milder condition compared to the classic photo-Fenton process.

Keywords: caffeine photodegradation; bio-based substances; Fenton; photo-Fenton, magnetic nanoparticles; urban waste

Introduction.

In recent years the organic fraction of urban waste (urban bio-waste, UBW) has attracted the attention of scientists as well as Institutions and policy makers, driven by the need of reducing society climate footprint and other environmental burdens, of achieving a more secure supply of resources and of boosting the bio economy (O'Callaghan 2016 and references therein). UBW can indeed be considered not only as a possible source of energy and/or fuel, rather as feedstock for the production of chemicals, inside the so-called biorefinery, a facility that integrates physical, chemical, biochemical and thermochemical processes to efficiently convert biomass feedstock. In this respect, biorefinery allows the valorization of bio-waste beyond energy applications.(Satchatippavarn et al. 2016; Gonzalez-García et al. 2016; Girotto et al. 2015). The feasibility of bio-waste upgrading has been investigated through several European projects (Biochemenergy, Biocore-europe, biowaste4sp, eurobioref). Among different approaches, in the present work we focused on waste-derived bio-based substances isolated from UBW, anaerobically and/or aerobically treated, following the findings of Montoneri et al. (Montoneri et al. 2011; Montoneri et al. 2013). They isolated several bio-based substances (hereinafter BBS) and characterized them under structural and physico-chemical point of view, evidencing the similarity between BBS and soil humic substances (Montoneri et al. 2011). Basically, BBS have been described as supramolecular aggregates with a complex lignin-derived structure containing several functionalities (namely, acid and basic functional groups bonded to aromatic and aliphatic chains); moreover the presence of both hydrophilic and hydrophobic moieties confers to BBS amphiphilic properties. Figure 1 is a schematic representation of the BBS isolation process and of the state of the art concerning their applications.

Among the wide range of BBS applications, the "waste for cleaning waste" approach has deserved great attention (Avetta et al. 2013). It consists in the use of BBS as chemical auxiliaries to drive photochemical degradation of pollutants. Actually it has been already demonstrated the capability of BBS to sensitize the photodegradation of phenols, azo-dyes and emerging pollutants through different mechanisms: i) direct sensitization, upon UV-VIS irradiation, by means of reactive oxygenated species production or excited triplet state formation; ii) auxiliaries in mild photo-Fenton like processes (Canonica et al. 1995; Wenk et al. 2011; Bianco Prevot et al. 2011; Gomis et al. 2015; Carlos et al. 2012).

Recently, attention has been paid to the heterogeneization of the BBS, by synthesizing hybrid magnetite-BBS nanoparticles (Magnacca et al. 2014). Magnetite (Fe_3O_4) nanoparticles represent promising candidates as catalysts for advanced oxidation processes (AOP) due to their benign nature and low-cost; furthermore, their properties can be tailored according to their purpose. Finally, the nanoparticles surface can be functionalized with a wide variety of non-toxic materials containing (photo)active groups that act both as stabilizers against the magnetite oxidation and also as catalysts (Nadejde et al. 2015; Nadejde et al. 2015a). In addition magnetite-organic hybrid materials are easy to be recovered from the solutions after their purification treatment (Munoz et al. 2015).

In the present work, a peculiar BBS fraction (namely BBSs) has been studied as photosensitizing agent; BBSs is soluble in all the pH range, whereas BBS typically precipitate at pH lower than about 3; under the solubility point of view BBSs can be considered more similar to the fulvic fraction of the natural organic matter, while BBS are similar to the humic one. Data previously obtained about the BBSs fraction indicated that BBSs aggregates have lower hydrodynamic radius than BBS ones, reduced aromaticity and higher concentration of carboxylic groups, thus yielding to higher hydrophilicity (Avetta et al. 2015).

The attention has been focused on the application of BBSs to the photodegradation of caffeine, chosen as representative compound among the so-called emerging pollutants present in aqueous solution. Caffeine is a psychoactive substance, widely consumed either for beverages or for pharmaceuticals and personal care products; it has been detected in natural water streams (Metcalfe et al. 2003) over many different countries, being not fully degraded in biological water treatment plants. Moreover caffeine has been considered as a chemical marker for surface water pollution (Buerge et al. 2003). Caffeine degradation studies are already reported in literature using TiO_2 and photo-Fenton approaches under solar conditions (Bernabeu et al. 2011; Klamerth et al. 2010; Klamerth et al. 2009; Klamerth et al. 2010a), and the caffeine photolysis was also studied in the presence of added fulvic acid (Jacobs et al. 2012).

BBSs performances have been studied following two different approaches: i) homogeneous degradation process, using BBSs aqueous solution; ii) heterogeneous process, using unique hybrid BBSs-magnetite nanoparticles, (hereinafter BBSs-NPs). This work includes therefore the synthesis and characterization of BBSs-NPs.

Materials and methods

Reagents

Caffeine, CH_3OH, NaOH, NH_4OH and $FeCl_3$ where purchased from Aldrich; CH_3CN and HCl were purchased from Merck; H_2O_2, $HClO_4$ and $FeSO_4x7H_2O$ were purchased from Panreac. All reagents were used without further purification.

For the preparation of BBSs solution, the starting material called BBS-GC, isolated from urban biowastes sampled from the process lines of ACEA Pinerolese Industriale S.p.A. waste treatment plant in Pinerolo (Italy), has been chosen. The urban biowaste was obtained in the compost production section, from urban public park trimming and home gardening residues aged for more than 180 days (green compost, GC). The process is an advanced system that comprises specific technological facilities, developed by ACEA Pinerolese Industriale S.p.A, and under European validation. Isolation of

BBS-GC was performed following a previously reported procedure (Nisticò et al. 2015). The BBSs fraction has been isolated in solution, after precipitation of the insoluble fraction at pH =1.5 with HCl.

Hybrid BBSs-NPs have been synthesized following a procedure reported in the literature (Magnacca et al. 2014, Cesano et al. 2015). In details, 3.7 g of $FeCl_3$ and 4.17 g of $FeSO_4x7H_2O$ (molar ratio Fe(III)/Fe(II) = 1.5) were dissolved in 100 mL of deionized water and heated up to 90°C. Once the temperature was reached, two solutions were added in sequence: a) 10 mL of 25 vol.% ammonium hydroxide, and b) 50 mL of a previously prepared BBSs aqueous solution. The mixture was mechanically stirred at 90°C for 30 min and then cooled down to room temperature. In this way a dispersion of BBSs-NPs has been directly obtained in a one-step process by co-precipitation method. Such dark-brown materials were washed twice with deionized water, deposited onto glass Petri dishes, and oven-dried at 80°C overnight.

Instrumental aspects

Fourier transform infrared (FTIR) spectra were recorded in transmission mode using the sample dispersed in KBr (1:20 weight ratio) by means of a Bruker Vector 22 spectrophotometer equipped with Globar source, DTGS detector, and working with 128 scans at 4 cm^{-1} resolution in the 4000-400 cm^{-1} range.

X-ray diffraction (XRD) patterns were obtained by using an X'Pert PRO MPD diffractometer from PANalytical, in Bragg-Brentano geometry in a flat sample-holder, equipped with Cu anode, working at 40 kV and 30 mA. The acquisition was performed in a 0.002° interval steps, with 45 s $step^{-1}$ in order to improve the signal to noise ratio. The magnetite particles size was also estimated by means of the Scherrer equation (Equation 1):

$$\tau = K\lambda/(\beta\cos\theta) \qquad (1)$$

where τ is the mean size of the crystalline domains (expressed in nm), K is a shape factor (typical value adopted for symmetrical shaped particles is 0.9), λ is the X-ray wavelength (0.154 nm), β is the line broadening at half the maximum intensity (FWHM) of the selected Bragg angle (expressed in radians), and θ is the Bragg angle (expressed in radians). For the magnetite NPs size quantification, the Bragg angle selected is the magnetite reflection (311) at ca. $2\theta = 35.6°$.

Thermo-gravimetric analyses (TGA) were carried out by means of TGA Q600 (TA Instruments). The powders (ca. 30 mg) were placed in an open alumina pan and heated from 40 to 800°C at the rate of 10°C min^{-1} under either nitrogen or air atmosphere. In order to calculate the organic fraction in the BBSs-NPs, the following equation was applied to the TGA results carried out in oxygen:

$$wt.\%_{om} = [wt.\%(T)_{150°C}] - [wt.\%(T)_{500°C}] \qquad (2)$$

Where: $wt.\%_{om}$ is the percent mass content of organic matter, $wt.\%(T_{150°C})$ is the initial percent dried mass content of the sample, and $wt.\%(T_{500°C})$ is the percent mass content before any Fe-involved transition.

Magnetization measurements were carried out with a LakeShore 7404 vibrating sample magnetometer. The hysteresis loop of the samples was registered at RT as the magnetic field was cycled between -20000 and 20000 Gauss.

Total organic carbon (TOC) content was determined by means of a ShimadzuTOC-VCSH analyzer. Measurements of pH were performed using a Methohm 713 pH-meter equipment with a combined glass electrode. ICP-OES, Perkin Elmer, Optima 5300 DV with cross-flow nebulizer was used for iron determination, with the following set-up: Argon C-45 (99.995% purity). 1300 W, gas plasma =15 L/min, auxiliary gas = 0.2 L/min, nebulizing gas = 0.8 L/min, sampling flow rate = 1.1 mL/min.

Caffeine was determined with a UHPLC Flexar FX-10, equipped with a S200 KIT-1022 PLUS autosampler, two Flexar FX 10 UHP PUMP MASTER pumps, FL degaser and a UV/VIS KIT-UHPLC detector. A Brownlee Analytical DB C18 column (30 mm length, i.d. 2.1 mm, particle diameter 1.9 μm) was used. CH_3CN (ACN) and water were used as eluent

A and B respectively, upon the following elution conditions: t = 0.0 min, A: 10%; t = 2.5 min, A:70%; t = 4.0 min, A: 3%. Eluent flow = 0.3 mL/min; detection wavelength = 205 nm.

Irradiation devices

Two different irradiation devices have been used throughout the work:

i) open solar simulator ORIEL INSTRUMENTS 81160 equipped with a Xenon lamp (300 W), whose emission spectrum closely matched the solar one; a cut off Pyrex filter was employed to filter the small fraction of photons emitted below 300 nm. Experiments were performed on 250 mL of solution, kept under magnetic stirring. Water was eventually added to compensate for the evaporation loss.

ii) Cylindrical Pyrex reactor equipped with a Xenon UV-TXE150 PESCHL ADVANCED lamp (150 Watt). Experiments were performed on 250 mL of solution under continuous oxygen bubbling (1 L/min flow rate).

The first set-up was used in the BBSs mediated photo-Fenton, while the second one was employed when nanoparticles were involved in order to allow air bubbling into the sample to keep the particles in suspension.

Results and discussion

Preliminarily TOC measurements have been performed on a BBSs solution isolated from an initial aqueous solution of 500 mgL^{-1} of BBS-GC. The obtained TOC average value was 45.1 ±0.4 mgL^{-1}, corresponding to 9.3 wt.% of the original BBS-GC. From this solution, aliquots have been properly diluted with water, in order to obtain the desired BBSs concentration, expressed as mgL^{-1} of organic C. For the experiments performed with BBSs, the TOC has indeed been taken as reference parameter in order to compare experiments run in different conditions.

Moreover, since BBS-GC powder presents 0.77±0.04 weight % of iron (Nisticò et al. 2015), this element was determined in the BBSs solution obtained from the BBS-GC initial solution, giving a value of 1.23±0.05 mgL^{-1}.

BBSs-NPs characterization

In order to better understand the chemical composition of BBSs-NPs, a wide physico-chemical characterization has been realized and data summarized in Figure 2.

Infrared spectroscopy was used to investigate the presence of BBSs in BBSs-NPs and the spectra are reported in Figure 2A. In particular, the presence of magnetite phase is highlighted by signals at 575 and 620 cm^{-1} due to Fe-O stretching vibrations, the presence of BBSs is confirmed by the BBSs-carboxylate stretching mode at ca. 1600 cm^{-1} (Magnacca et al. 2014), the signal at 1120 cm^{-1} is due to C-O stretching mode of organic matter adsorbed onto the iron oxide surface (i.e. polysaccharides and other BBS-derived substances) (Ou et al. 2009) and the very sharp band at 1400 cm^{-1} witnessed the interaction between BBSs-carboxylate functionalities and the iron oxide surface (Ou et al. 2009). No evidence of iron/iron oxide present as impurities in BBS-GC (used to prepared the BBSs) is observed in the spectrum since the organic matter modes hidden all the possible present signals.

Thermogravimetric analyses have been performed in order to assess the BBSs-NPs stability as well as the organic matter content. Figure 2B reports the profiles obtained working under air (oxidant) or nitrogen (inert/reducing) atmosphere. The thermal profile of BBSs-NPs treated in air (black curves in Figure 2B) shows three weight losses, as clearly evidenced by the DTG curve: the first one, in the range 30-150°C, corresponding to water evaporation; the second one, complex, in the range 150-500°C, corresponding to BBSs oxidation to CO_2 and the third one, at temperatures higher than 600°C, that can be assigned to the magnetite to hematite transition. In spite of the Curie temperature reported for this transition (i.e. 580°C), a peak is observed at T > 600°C, suggesting a protection role of the organic matter towards magnetite oxidation, since the phase transformation occurs only after the complete removal of the organic matter. Vice versa, when TGA was

run under N_2 atmosphere (red curves in Figure 2B), the main difference concerned the transformation of the BBSs, which is a three steps process. As evidenced by the DTG profile, the three maxima at ca. 230, 310 and 430°C correspond to the degradation of the ammonium-containing salts (at ca. 230°C), and the pyrolysis of the BBSs carbohydrate fraction (at ca. 310°C, according to FTIR results) and the BBSs lignin-like fraction (at ca. 430°C), thus yielding to the formation of a carbonaceous residue (Ou et al. 2009, Franzoso et al. in preparation). Additionally, the transition magnetite to wustite, which is a diamagnetic iron oxide (FeO), at ca. 720°C is also registered. Since at the end of TGA analysis the material is still magnetic, it can be hypothesized that wustite disproportionate giving magnetite and zero valent iron (both magnet-sensitive iron-containing phases) (Cesano et al. 2015).

Basing on TGA experiments performed on BBSs-NPs in oxygen flux, the amount of BBSs present in the hybrid BBSs-NPs can be estimated by means of weight loss in the range 150-500°C, following the Equation 2. The calculated amount corresponded to 14.2 wt.% of organic matter.

The presence of magnetite forming the BBSs-NPs was identified through XRD (see Figure 2C). All the crystalline reflections in the figure at 2θ = 30.1° (220), 35.4° (311), 43.0° (400), 53.9° (422) 57.2° (511), and 62.6° (440) are consistent with the neat magnetite phase. No relevant reflections are expected from BBSs since its XRD pattern presents only one broad amorphous contribution centered at ca. 2θ = 25° and few negligible signals (Franzoso et al. in preparation). Extra peaks (the main relevant one at ca. 2θ = 32.5°) are due to by-products (mainly ammonium-containing salts) of the coprecipitation reaction for the magnetite synthesis. Scherrer formula applied to the (311) magnetite signal was used to estimate the average BBSs-NPs size. The calculated value corresponded to ca. 16.7 nm.

The magnetic properties of both BBSs-NPs and neat magnetite are reported in Figure 2D. In general, both samples reveal superparamagnetic behaviors, with negligible remanence and very low coercitivity (< 10 G). The values of saturation magnetization of BBSs-NPs was 47 emu g^{-1}, slightly lower than neat magnetite (64 emu g^{-1}). This behavior suggests a different amount of magnetite per gram of sample due to the presence of the BBSs covering shell (Cesano et al. 2015; Franzoso et al. in preparation).

Caffeine photodegradation.

BBSs

A previous study reported in the literature showed a negligible caffeine photodegradation (5% of caffeine abatement after 8 hours irradiation) due only to light irradiation, when using the same experimental set-up (Gomis 2014).

In the present research 5 mg L^{-1} of caffeine have been firstly irradiated for three hours in the presence of BBSs at a concentration corresponding to 5 mg L^{-1} of organic C (about 54 mg L^{-1} BBSs), at pH= 5.0. As can been observed in Fig.3 the abatement of caffeine was negligible after 2 hours of irradiation.

Further experiments have been performed in the same experimental conditions but adding H_2O_2 7.5x 10^{-4} M. This is the stoichiometric amount of hydrogen peroxide required to mineralize the caffeine present in the sample; under these conditions, 85% of caffeine abatement was attained after two hours of irradiation.

As it clearly appears in the Figure 3, the irradiation of caffeine solution in the presence of the H_2O_2 alone, in the absence of BBSs, yields to a worst degradation efficiency, underlying a synergistic effect of H_2O_2 and BBSs on the process. It could be hypothesized that BBSs sensitizes the $^{\bullet}OH$ radicals generation from H_2O_2 and/or a photo-Fenton-like process occurs in the BBSs solution, due to presence of iron even if at very low concentration.

Based on these results and on previously reported evidences of the capability of bio-based substances to complex iron ions yielding to experimental conditions similar to the ones applied in photo-Fenton process (Pignatello 2006, Ou, 2007, Sulzberger 2015), further experiments have been performed adding iron salts. It is worth to be noticed that all the

experiments have been run at pH=5.0, whereas lower pH values are usually required as optimum conditions, due to the low solubility of Fe(III) at mild pH. This pH has been chosen because in previous papers it was determined as the highest value where photo-Fenton can be run in the presence of BBS with an acceptable loss of efficiency, as pH closer to neutrality resulted to be inconvenient (Gomis et al., 2015).

Figure 4 shows the results obtained by irradiating the caffeine aqueous solution in the presence of BBSs, 7.5×10^{-4} M of H_2O_2 and 5.0 mg L^{-1} of Fe(II), at pH = 5. For the sake of comparison, the results obtained by operating in the dark, adopting the same experimental conditions are also reported.

It clearly appears that the addition of Fe(II) induces both Fenton and photo-Fenton-like degradation processes, yielding to the 40% and to the 80% of caffeine disappearance, respectively, after 15 minutes of reaction. It is interesting to note that the initial reaction rate is similar in both cases (Fenton process) but after 2 minutes, the Fenton process results clearly slower than photo-Fenton. The pH modification was negligible along the experiments, as final values were systematically above 4.5.

The effect of iron concentration has been explored for the photo-Fenton-like process; experiments results are shown in Figure 5. Only in the presence of Fe(II) at 4 and 5 mg L^{-1}, after 5 min of irradiation a dark precipitate has been observed, probably due to iron oxides precipitation. Compared to the caffeine degradation performed in the presence of H_2O_2 alone, the addition of Fe(II) starts to affect the degradation rate at concentration higher than 2 mg L^{-1}. Under the applicative point of view, the gain in terms of degradation rate upon addition of iron salt, cheap and non-toxic substance, compensates the cost increase. However, further addition of this metal is not always convenient, as it is limited by legislation.

In the presence of 5 mg L^{-1} of added Fe(II) the effect of pH has also been checked by performing several experiments in the pH range from 2.8 to 5.0 and the best performances have been obtained at pH=3.9 that is probably the best compromise between reactive species production and Fe(III) stabilization by BBSs (Figure 1S in the supplementary material). Shift of the optimum pH towards slightly acidic values was already reported (Gomis et al. 2015) and variation of the key species driving the photodegradation process was hypothesized. While $Fe(OH)^{2+}$ is considered the specie responsible when the optimum results are obtained at pH = 2.8, a relevant role was attributed to photoactive Fe(III)-BBS complexes when the best results were obtained at pH about 4. Moreover, when ethylenediamine-N,N-disuccinic acid was used as iron complexing agent (Huang et al., 2013), the best results were reached at neutral or even slightly basic medium and it was proposed a completely different mechanism, in which superoxide played a key role.

However, the complexity of the system makes difficult to find clear evidence for this mechanistic issue.

The BBSs concentration was then decreased down to 0.9 mg L^{-1} as organic C; in the absence of added iron some degradation of caffeine was observed. This could be attributed to two different reasons: a) the photosensitizing effect of BBSs that is able to catalyze decomposition of hydrogen peroxide into $^{\bullet}OH$ radicals and b) the small amount of iron originally present in BBSs solution that could drive at certain extent a photo-Fenton process (Gomis et al., 2013). However, caffeine degradation efficiency increased upon iron addition (Figure 6); this evidence allows to hypothesize that, in the presence of added iron, the main effect of BBSs is due to its capability to stabilize iron ions in solution at mild pH, allowing the Fenton-like process to take place. In this case the minimum amount of added BBSs able to stabilize iron ions in solution is enough, and reduces the competition for light harvesting; on the opposite side, in the absence of added iron, if the photosensitization is mainly related to reactive species production assisted by irradiated BBSs, an increase in BBSs concentration favors the process. Furthermore, BBS also plays a competitive role for H_2O_2 which could be expected to be more significant in the case of photo-Fenton process, which is more efficient than BBSs sensitization.

Regarding to the environmental problems associated to the addition of BBS to the effluent, previous results showed that the toxicity of these substances at the concentration employed in this work (few mg L^{-1}) is negligible, according to

different bioassays (Gomis et al, 2015b). Hence, although it could be a concern if the treated water is designated to human consumption, this should not be a problem when discharged in ecosystems, because of BBSs biocompatibility and similarity between BBSs and humic substances that constitute the major fraction of natural organic matter.

BBSs-NPs

Caffeine photodegradation in the presence of BBSs-NPs has been studied in a Pyrex reactor under continuous air bubbling, to guarantee the suspension stirring; the obtained results are reported in Figure 7. Preliminarily, the absence of caffeine direct photolysis has been verified; then caffeine degradation experiments have been performed under light irradiation, in the presence of 200 mg L^{-1} of BBSs-NPs. Based on TGA results, a corresponding BBSs content of about 30 mgL^{-1}can be roughly estimated, that is in the same order of magnitude than the BBSs concentration employed in homogeneous tests; analogously to what observed in the homogeneous system, caffeine degradation was negligible (data not reported). On the opposite, when adding H_2O_2 alone (blue squares in Fig.7) about 70% of caffeine abatement was attained after 30 min of irradiation; the generation of •OH radicals through H_2O_2 photolysis could be invoked, as in the case of tests performed in the open reactor, previously discussed. The different degradation kinetics observed in the two reaction devices could be reasonably ascribed to reactor geometry and dissolved oxygen content (L. Santos-Juanes et al., 2011).

The highest caffeine degradation efficiency has been reached in the presence of BBSs-NPs, H_2O_2 and Fe(II), both in the dark and under light irradiation; the total substrate disappearance occurred in both cases after 7 min of contact time. This result is apparently in contrast to what observed working with BBSs in homogeneous system, where the process was rather faster under light irradiation. An explanation could be found in the role played by i) the magnetite present in the BBSs-NPs structure, and ii) the high oxygen concentration. Indeed it has been demonstrated (Nadejde et al., 2015) that magnetite nanoparticles mediate the production of radicals from H_2O_2 decomposition and that the phenomenon is not hindered by coating the iron oxide core with organics. On the other hand, magnetite could activate molecular oxygen via single-electron reduction pathway to produce reactive oxygen species. Both mechanisms are effective also in the dark and this should explain why no significant caffeine degradation improvement has been observed under light irradiation. In any case, due to its complexity, the BBSs-NPs working mechanism deserves further investigation.

Conclusions

The obtained results show the viability of photodegradation of caffeine assisted by waste derived bio-based materials (BBSs). In particular, both homogeneous and heterogeneous systems are promising approaches to drive photo-Fenton processes under mild pH, which results in an enhanced sustainability of the process. It can therefore be concluded that biowaste are worth to be considered as a green tool for the preparation of materials for water treatments.

Acknowledgements

This work was performed with the financial support for academic interchange by the Marie Sklodowska-Curie Research and Innovation Staff Exchange project funded by the European Commission H2020-MSCA-RISE-2014 within the framework of the research project Mat4treaT (Project number 645551). Compagnia di San Paolo and University of Torino are gratefully acknowledged for funding Project Torino_call2014_L2_126 through ‘‘Bando per il finanziamento di progetti di ricerca di Ateneo – anno 2014’’ (Project acronym: Microbusters). Additionally, authors would like to acknowledge Dr. Flavio R. Sives (La Plata, Argentina) for magnetization measurements.

References

Avetta P, Bella F, Bianco Prevot A, Laurenti E, Montoneri E, Arques A, Carlos L, (2013) Waste cleaning waste: photodegradation of monochlorophenols in the presence of waste derived organic catalysts. ACS Sustainable Chemistry & Engineering 1: 1545–1550

Avetta P, Berto S, Bianco Prevot A, Minella M, Montoneri E, Persico D, Vione D, Gonzalez MC, Mártire DO, Carlos L, Arques A, (2015) Photoinduced transformation of waste-derived soluble bio-based substances. Chemical Engineering Journal 274: 247-255

Bernabeu A, Vercher RF, Santos-Juanes L, Simón PJ, Lardín C, Martínez MA, Vicente JA, González R, Llosá C, Arques A, Amat AM, (2011) Solar photocatalysis as a tertiary treatment to remove emerging pollutants from wastewater treatment plant effluents. Catalysis Today 161: 235–240

Bianco Prevot A, Avetta P, Fabbri D, Laurenti E, Marchis T, Perrone DG, Montoneri E, Boffa V, (2011) Waste derived bio-organic substances for light induced generation of reactive oxygenated species. ChemSusChem, 4: 85-90

Buerge IJ, Poiger T, Müller MD, Buser HR, (2003) Caffeine, an anthropogenic marker for wastewater contamination of surface waters. Environmental Science and Technology, 37: 691–700

Canonica S, Jans U, Stemmler K, Hoigné J, (1995) Transformation kinetics of phenols in water: photosensitization by dissolved natural organic material and aromatic ketones. Environ. Sci. Technol. 29: 1822-1831

Carlos L, Martire DO, Gonzalez MC, Gomis J, Bernabeu A, Amat AM, Arques A, (2012) Photochemical fate of a mixture of emerging pollutants in the presence of humic substances. Water research 46: 4732-4740

Cesano F, Fenoglio G, Carlos L, Nisticò R, (2015) One-step synthesis of magnetic chitosan polymer composite films. Applied Surface Science 345: 175-181.

Girotto F, Alibardi L, Cossu R, (2015) Food waste generation and industrial uses: A review. Waste Management 45: 32–41

Gomis J, Vercher RF, Amat AM, Martire DO, González MC, Bianco-Prevot A, Montoneri E, Arques A, Carlos L (2013). Application of soluble bio-organic substances (SBO) as photocatalysts for wastewater treatment: sensitizing effect and photo-Fenton-like process. Catalysis Today, 209, 176-180.

Gomis J, Bianco Prevot A, Montoneri E, Gonzalez MC, Amat AM, Martire DO, Arques A, Carlos L, (2014) Waste sourced bio-based substances for solar-driven wastewater remediation: Photodegradation of emerging pollutants. Chemical Engineering Journal 235: 236-243

Gomis J, Carlos L, Bianco Prevot A, Teixeira ACSC, Mora M, Amat AM, Vicente R, Arques A, (2015) Bio-based substances from urban waste as auxiliaries for solar photo-Fenton treatment under mild conditions: Optimization of operational variables. Catalysis Today 240 39-45

Gomis J, Gonçalves MG, Vercher RF, Sabater C, Castillo MA, Bianco Prevot A, Amat AM, Arques A. (2015b) Determination of photostability, biocompatibility and efficiency asphoto-Fenton auxiliaries of three different types of soluble bio-based substances (SBO). Catalysis Today 252, 177–183

Gonzalez-García S, Gullon B, Rivas S, Feijoo G, Moreira MT, (2016) Environmental performance of biomass refining into high-added value compounds. Journal of Cleaner Production 120: 170-180

http://costeubis.org/ last accessed May 2016

Huang W, Brigante M, Wu F, Mousty C, Hanna K, Mailhot G, (2013) Assessment of the Fe(III)-EDDS complex in Fenton-like processes: from the radical formation to the degradation of Bisphenol A Environ. Sci.Technol. 47: 1952–1959

Jacobs LE, Weavers LK, Houtz EF, Chin Y, (2012) Photosensitized degradation of caffeine: Role of fulvic acids and nitrate. Chemosphere 86: 124–129

Klamerth N, Miranda N, Malato S, Agüera A, Fernández-Alba AR, Maldonado MI, Coronado JM, (2009) Degradation of emerging contaminants at low concentrations in MWTPs effluents with mild solar photo-Fenton and TiO_2. Catalysis Today 144: 124–130

Klamerth N, Malato S, Maldonado MI, Agüera A, Fernández-Alba AR, (2010) Application of photo-Fenton as a tertiary treatment of emerging contaminants in municipal wastewater. Environmental Science and Technology, 44: 1792–1798

Klamerth N, Rizzo L, Malato S, Maldonado MI, Agüera A, Fernández-Alba AR, (2010a) Degradation of fifteen emerging contaminants at mu g L-1 initial concentrations by mild solar photo-Fenton in MWTP effluents. Water Research, 44: 545–554

Magnacca G, Allera A, Montoneri E, Celi L, Benito DE, Gagliardi LG, Gonzalez MC, Mártire DO, Carlos L, (2014) Novel magnetite nanoparticles coated with waste-sourced biobased substances as sustainable and renewable adsorbing materials. ACS Sustainable Chem. Eng. 2 (6): 1518–1524

Metcalfe CD, Miao XS, Koenig BG, Struger J, (2003) Distribution of acidic and neutral drugs in surface waters near sewage treatment plants in the lower Great Lakes, Canada. Environmental Toxicology and Chemistry 22: 2881–2889

Montoneri E, Mainero D, Boffa V, Perrone DG, Montoneri C, (2011) Biochemenergy: a project to turn an urban wastes treatment plant into biorefinery for the production of energy, chemicals and consumer's products with friendly environmental impact. Int. J Global Environ Issues 11: 170-196

Montoneri E, Bianco Prevot A, Avetta P, Arques A, Carlos L, Magnacca G, Laurenti E, Tabasso S, (2013) Food wastes conversion to products for use in chemical and environmental technology, material science and agriculture. In: Kazmi A, Shuttleworth P (eds) The Economic Utilisation of Food Co-Products, Royal Society of Chemistry, pp.64-109

Munoz M, de Pedro ZM, Casas JA, Rodriguez JJ, (2015) Preparation of magnetite-based catalysts and their application in heterogeneous Fenton oxidation – A review. Applied Catalysis B: Environmental 176–177: 249–265.

Nadejde C. Neamtu M. Hodoroaba VD, Schneider RJ, Paul A, Ababei G, Panne U, (2015) Tannic acid- and natural organic matter-coated magnetite as green Fenton-like catalysts for the removal of water pollutants. J Nanopart Res 17: 476-486.

Nadejde C. Neamtu M. Hodoroaba VD, Schneider RJ, Paul A, Ababei G, Panne U, (2015a) Green Fenton-like magnetic nanocatalysts: Synthesis, characterization and catalytic application. Applied Catalysis B: Environmental 176–177: 667–677

Nisticò R, Barrasso M, Carrillo Le Roux GA, Seckler MM, Sousa W, Malandrino M, Magnacca G, (2015) Biopolymers from composted biowaste as stabilizers for the green synthesis of spherical and homogeneously sized silver nanoparticles for textile application on natural fibers. ChemPhysChem 16: 3902-3909

O'Callaghan K, (2016) Technologies for the utilisation of biogenic waste in the bioeconomy. Food Chemistry 198: 2–11

Ou X, Quan X, Chen S, Zhao H, Zhang Y, (2007) Atrazine photodegradation in aqueous solution induced by interaction of humic acids and iron: photoformation of iron(II) and hydrogen peroxide J. Agric. Food Chem. 55: 8650-8656

Ou X, Chen S, Quan X, Zhao H, (2009) Photochemical activity and characterization of the complex of humic acids with iron(III). Journal of Geochemical Exploration 102: 49-55

Pignatello JJ, Oliveros E, Mackay A, (2006) Advenced oxidation processes for organic contaminant destruction based on the Fenton reaction and related chemistry. Critical Reviews in Environmental Science and Tecnology 36: 1-84

Santos-Juanes L, García Sáncheza JL, Casas Lópeza JL, Oller I, Malato S, Sánchez Péreza JA, (2011) Dissolved oxygen concentration: A key parameter in monitoring the photo-Fenton process. Applied Catalysis B: Environmental 104: 316–323

Satchatippavarn S, Martinez-Hernandez E, Hang P, Leach M, Yang A, (2016) Urban biorefinery for waste processing. Chemical Engineering Research and Design 107: 81–90

Sulzberger B, (2015) Light-induced redox cycling of iron: roles for CO_2 uptake and release by aquatic ecosystems Aquat Geochem 21:65–80

Wenk J, Von Gunten U, Canonica S, (2011) Effect of dissolved organic matter on the transformation of contaminants induced by excited triplet states and the hydroxyl radical. Environ. Sci. Technol. 45: 1334-1340

http://www.biochemenergy.it/

www.biocore-europe.org, last accessed May 2016

www.biowaste4sp.eu, last accessed May 2016

www.eurobioref.org, last accessed May 2016

Figure captions

Figure 1. Schematic representation of BBS isolation and their tested applications.

Figure 2 Physicochemical characterization of reference neat BBSs and BBSs-NPs. Panel A: Absorbance FTIR spectra in the 1800-400 cm^{-1} range relative to neat magnetite (A, black solid line), BBSs-NPs (B, red solid line), and neat BBS (C, red dotted line). The main relevant peaks are labeled. All spectra are collected in transmission mode through KBr pellets. Panel B: TG (solid line) and DTG (dotted lines) curves of BBSs-NPs heated either in air (black) or in nitrogen (red) atmosphere. Panel C: XRD patterns of the neat magnetite (black) and BBSs-NPs (red). The main reflections due to magnetite are highlighted and labeled. Panel D: Magnetization curves evaluation of neat magnetite (black) and BBSs-NPs (red).

Figure 3 Relative caffeine concentration vs. irradiation time. Experimental conditions: caffeine at time 0, 5 mg L^{-1}, pH=5.0. Legends: Blue diamonds: BBSs 5 mg L^{-1} (as organic C). Black triangles: H_2O_2 7.5×10^{-4} M. Red squares: BBSs 5 mg L^{-1} (as organic C), H_2O_2 7.5×10^{-4} M.

Figure 4 Relative caffeine concentration vs. contact time. Experimental conditions: caffeine at time 0, 5 mg L^{-1}, pH=5.0, BBSs 5 mg L^{-1} (as organic C), H_2O_2 7.5×10^{-4} M, Fe(II) 5 mg L^{-1}. Legend: Blue triangles: Fenton experiments in the dark. Green triangles: photo-Fenton experiments under light irradiation.

Figure 5 Caffeine relative concentration vs. irradiation time. Experimental conditions: caffeine at time 0, 5 mg L^{-1}, pH=5.0, BBSs 5 mg L^{-1} (as organic C), H_2O_2 7.5×10^{-4} M. Effect of the Fe(II) concentration. Legend: Black squares: Fe(II) 1 mg L^{-1}. Red circles: Fe(II) 2 mg L^{-1}. Blue up-triangles: Fe(II) 3 mg L^{-1}. Dark cyan down-triangles: Fe(II) 4 mg L^{-1}. Magenta squares: Fe(II) 5 mg L^{-1}.

Figure 6. Caffeine relative concentration vs. irradiation time. Experimental conditions: caffeine at time 0, 5 mg L^{-1}, pH=5.0, H_2O_2 7.5×10^{-4} M. Red series: Solid squares, red solid line: BBSs 5 mg L^{-1} (as organic C); Open squares, dotted line: BBSs 0.9 mg L^{-1} (as organic C). Green series: Fe(II) 5 mg L^{-1}; Solid triangles, solid line: BBSs 5 mg L^{-1} (as organic C); Open triangles, dotted line: BBSs 0.9 mg L^{-1} (as organic C).

Figure 7. Caffeine relative concentration vs. contact time. Experimental conditions: caffeine at time 0, 5 mg L^{-1}, pH=5.0. Blue diamonds: H_2O_2 7.5×10^{-4} M. Red squares: H_2O_2 7.5×10^{-4} M, BBSs-NPs 200 mg L^{-1}. Green solid triangles: H_2O_2 7.5×10^{-4} M, BBSs-NPs 200 mg L^{-1}, Fe(II) 5 mg L^{-1}, photo Fenton experiments under light irradiation; Green open triangles: H_2O_2 7.5×10^{-4} M, BBSs-NPs 200 mg L^{-1}, Fe(II) 5 mg L^{-1}, Fenton experiments in the dark.

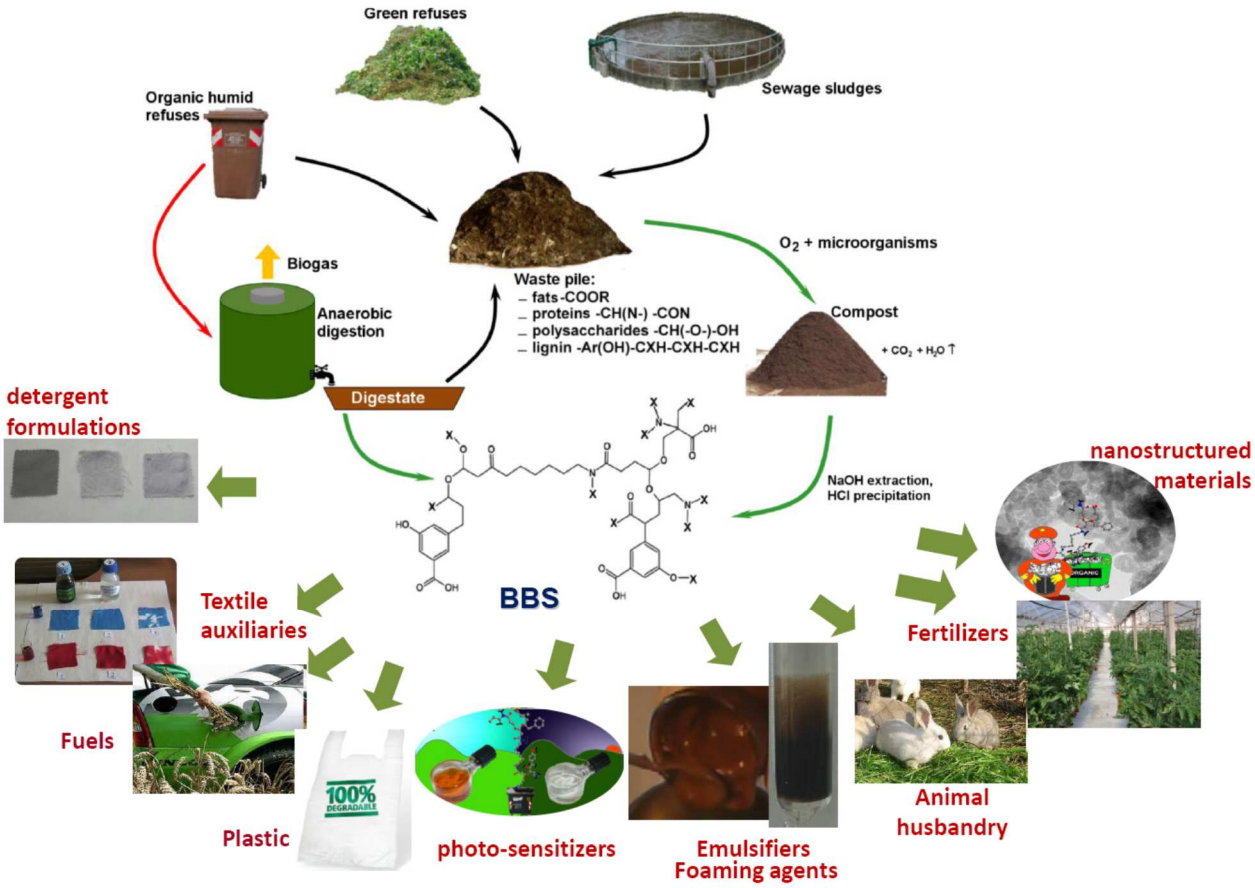
Green refuses
Sewage sludges
Organic humid refuses
Biogas
Anaerobic digestion
Digestate
Waste pile:
– fats-COOR
– proteins -CH(N-) -CON
– polysaccharides -CH(-O-)-OH
– lignin -Ar(OH)-CXH-CXH-CXH
O_2 + microorganisms
Compost
+ CO_2 + H_2O ↑
detergent formulations
NaOH extraction, HCl precipitation
nanostructured materials
BBS
Textile auxiliaries
Fertilizers
Fuels
Plastic
photo-sensitizers
Emulsifiers Foaming agents
Animal husbandry

Figure 1

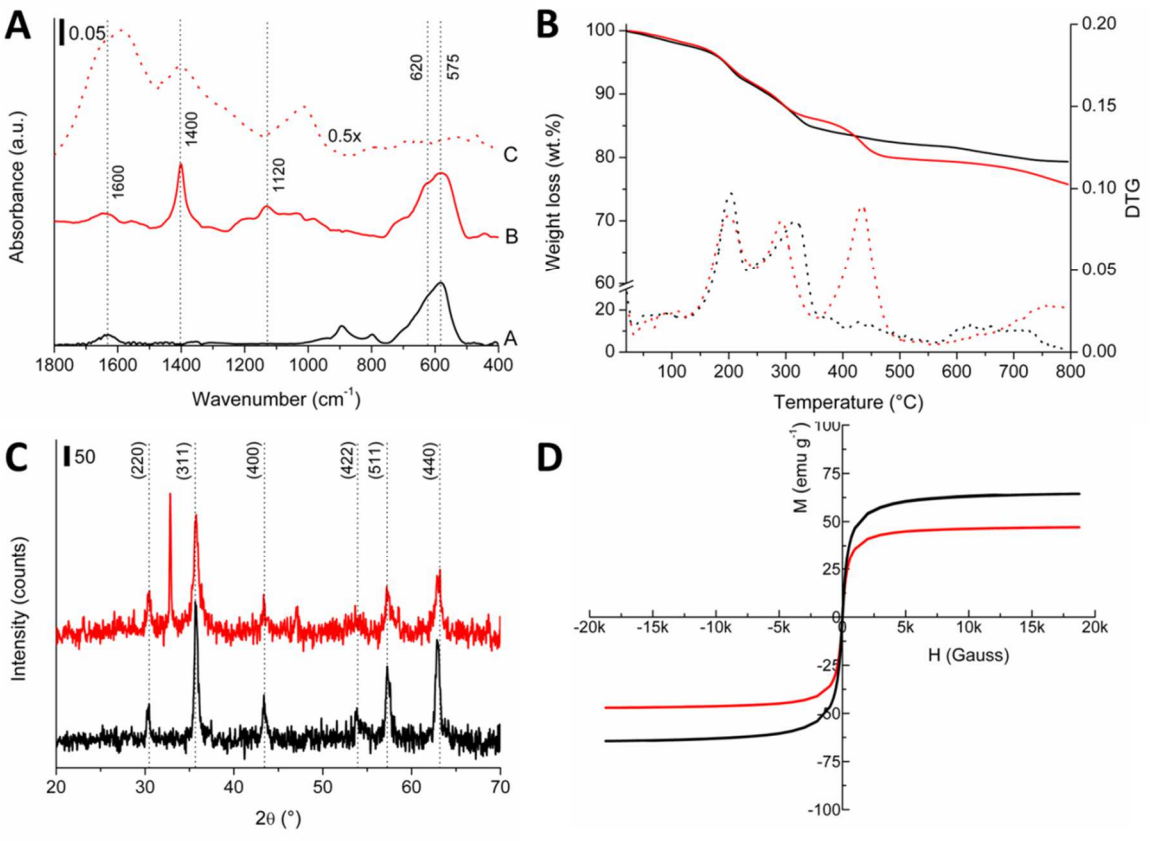
A
0.05
Absorbance (a.u.)
1600
1400
1120
620
575
0.5x
C
B
A
1800 1600 1400 1200 1000 800 600 400
Wavenumber (cm-1)
B
Weight loss (wt.%)
DTG
100 90 80 70 60 20 0
0.20 0.15 0.10 0.05 0.00
100 200 300 400 500 600 700 800
Temperature (°C)
C
50
Intensity (counts)
(220)
(311)
(400)
(422)
(511)
(440)
20 30 40 50 60 70
2θ (°)
D
M (emu g-1)
100 75 50 25 0 -25 -50 -75 -100
-20k -15k -10k -5k 0 5k 10k 15k 20k
H (Gauss)

Figure 2

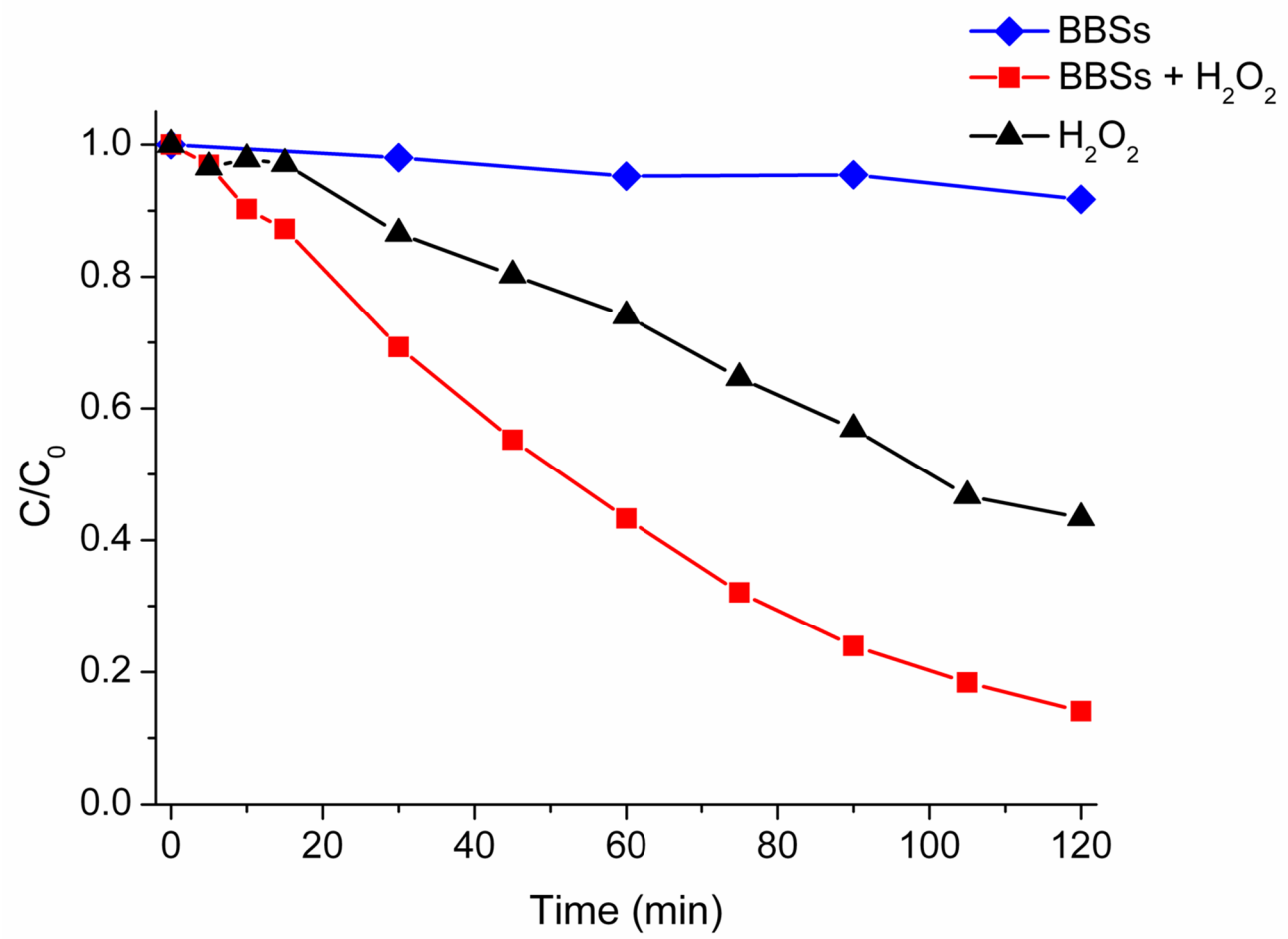
BBSs
BBSs + H2O2
H2O2
C/C0
1.0
0.8
0.6
0.4
0.2
0.0
0
20
40
60
80
100
120
Time (min)

Figure 3

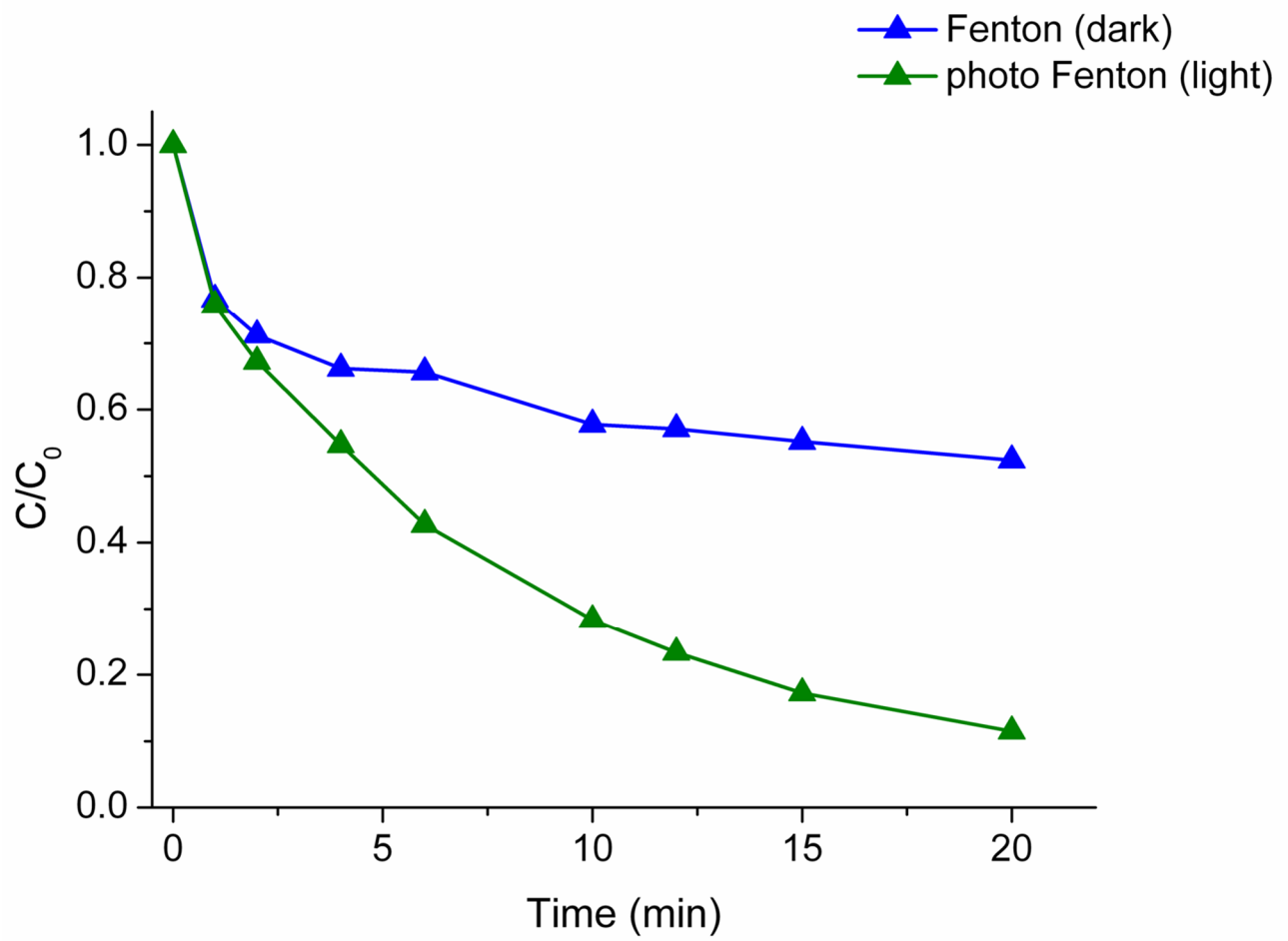
Fenton (dark)
photo Fenton (light)
1.0
0.8
0.6
0.4
0.2
0.0
C/C0
0
5
10
15
20
Time (min)

Figure 4

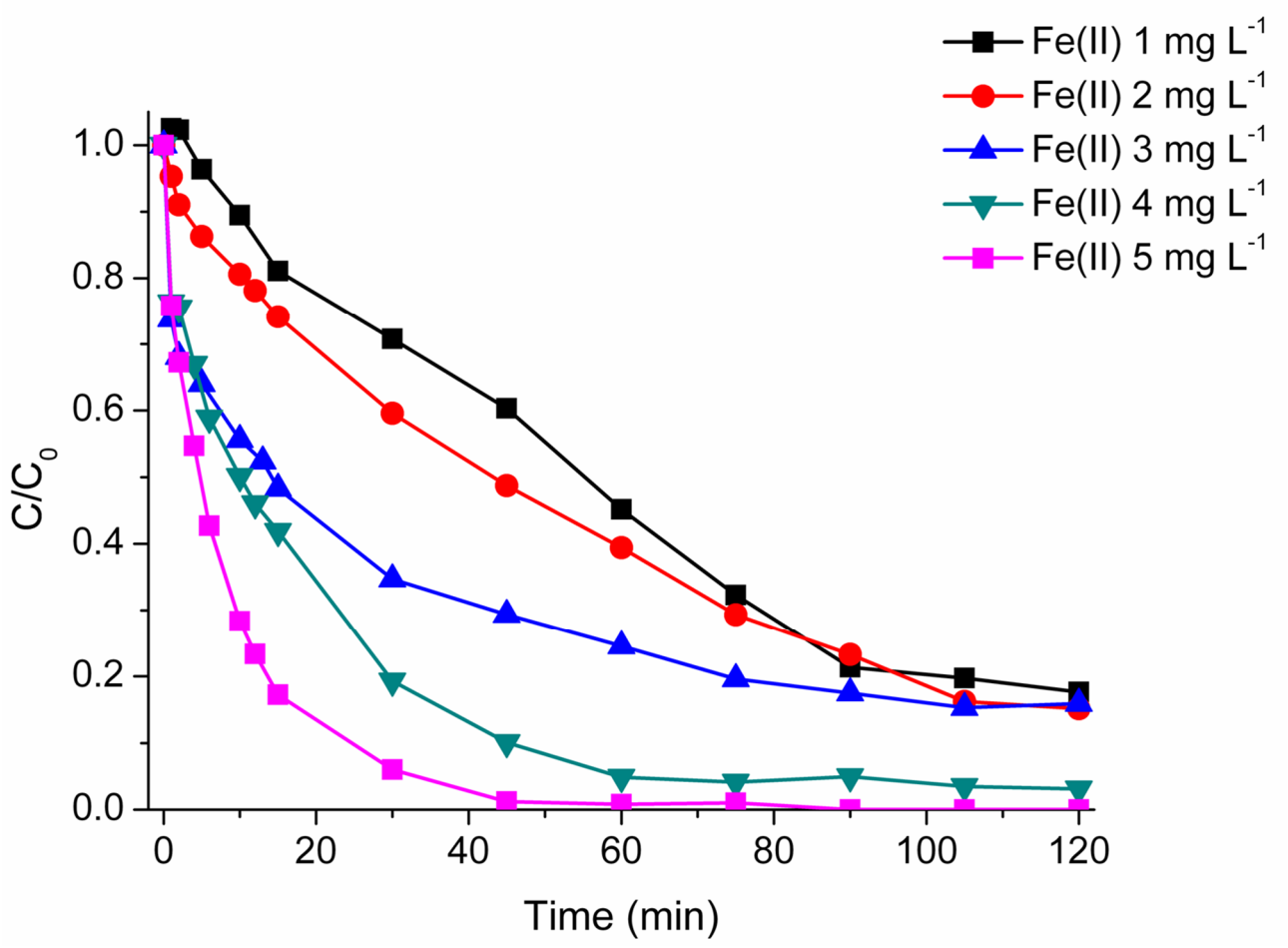
Fe(II) 1 mg L-1
Fe(II) 2 mg L-1
Fe(II) 3 mg L-1
Fe(II) 4 mg L-1
Fe(II) 5 mg L-1
C/C0
1.0
0.8
0.6
0.4
0.2
0.0
0
20
40
60
80
100
120
Time (min)

Figure 5

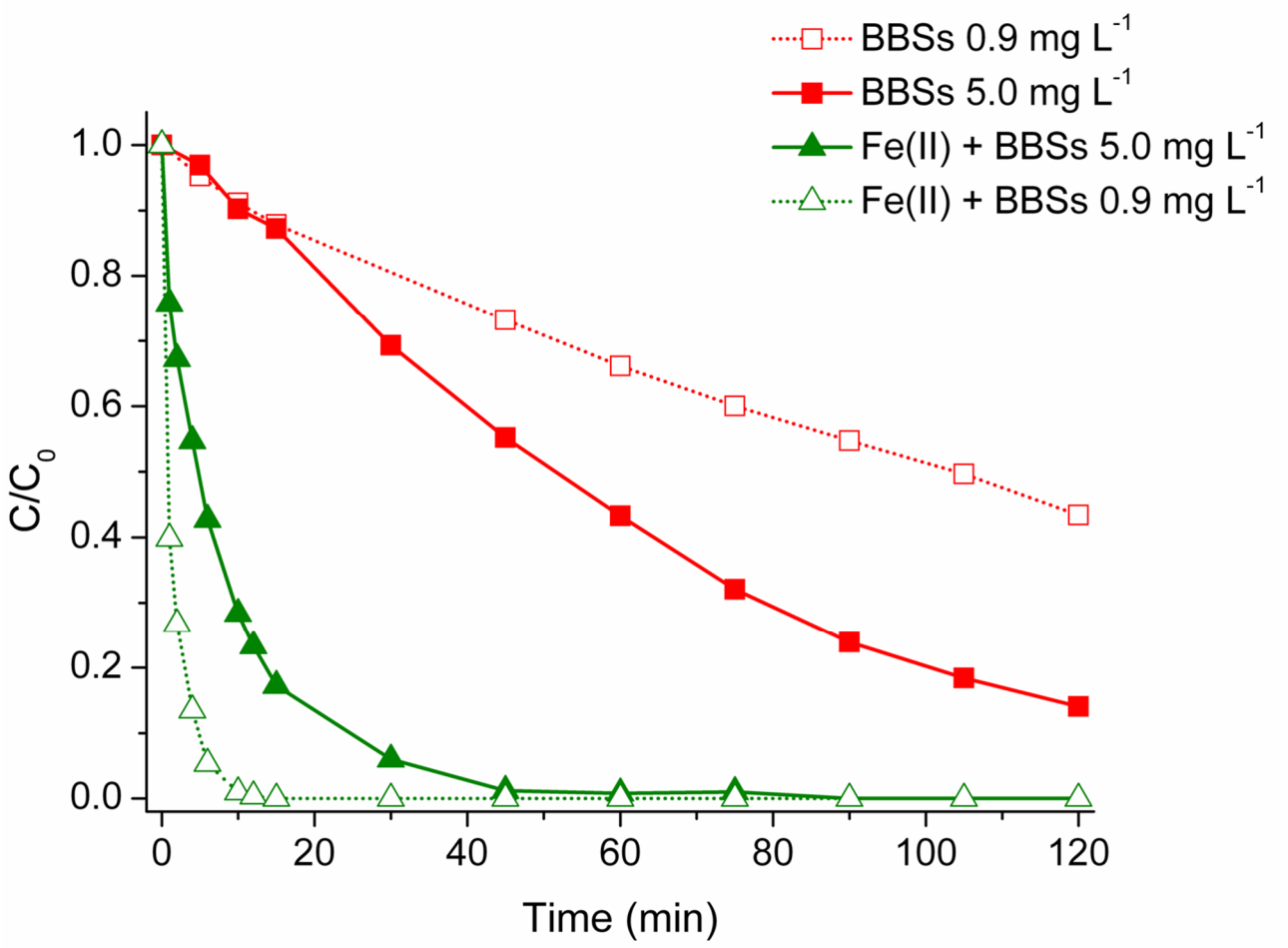
BBSs 0.9 mg L-1
BBSs 5.0 mg L-1
Fe(II) + BBSs 5.0 mg L-1
Fe(II) + BBSs 0.9 mg L-1
C/C0
1.0
0.8
0.6
0.4
0.2
0.0
0
20
40
60
80
100
120
Time (min)

Figure 6

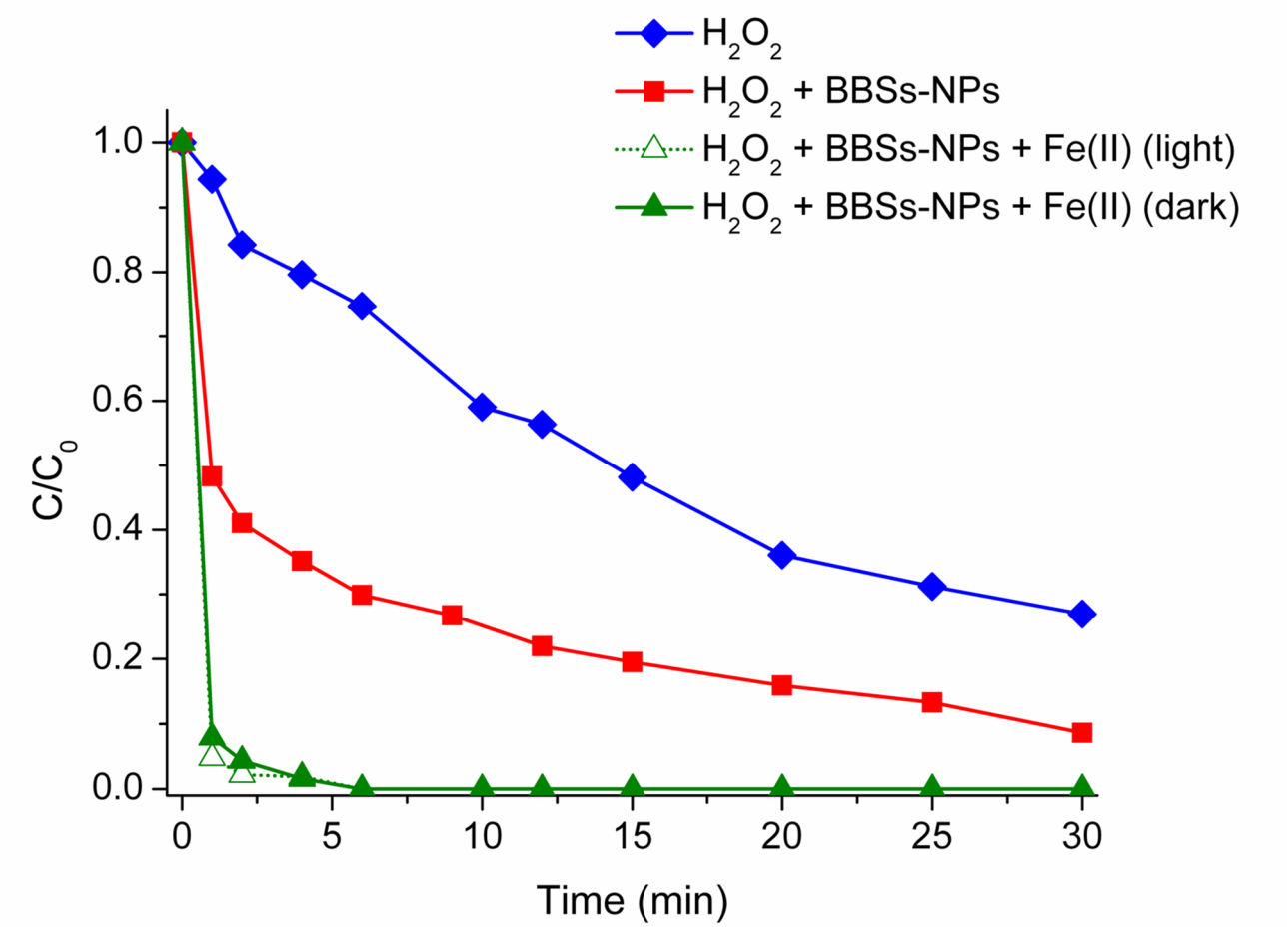
H2O2
H2O2 + BBSs-NPs
H2O2 + BBSs-NPs + Fe(II) (light)
H2O2 + BBSs-NPs + Fe(II) (dark)
C/C0
1.0
0.8
0.6
0.4
0.2
0.0
0
5
10
15
20
25
30
Time (min)

Figure 7